HOKKAIDO UNIVERSITY

Title	Photoredox Cascade Catalysts for Solar Hydrogen Production From Sustainable Hydrogen Sources
Author(s)	Kobayashi, Atsushi
Citation	ChemSusChem, 18(1), e202400688 https://doi.org/10.1002/cssc.202400688
Issue Date	2025-01-02
Doc URL	https://hdl.handle.net/2115/97353
Rights	This is the peer reviewed version of the following article: Photoredox Cascade Catalysts for Solar Hydrogen Production From Sustainable Hydrogen Sources / Kobayashi, Atsushi, which has been published in final form at https://doi.org/10.1002/cssc.202400688. This article may be used for non-commercial purposes in accordance with Wiley Terms and Conditions for Use of Self-Archived Versions. This article may not be enhanced, enriched or otherwise transformed into a derivative work, without express permission from Wiley or by statutory rights under applicable legislation. Copyright notices must not be removed, obscured or modified. The article must be linked to Wiley's version of record on Wiley Online Library and any embedding, framing or otherwise making available the article or pages thereof by third parties from platforms, services and websites other than Wiley Online Library must be prohibited.
Type	journal article
File Information	ChemSusChem18(1).pdf

Hokkaido University Collection of Scholarly and Academic Papers : HUSCAP

Photoredox Cascade Catalysts for Solar Hydrogen Production from Sustainable Hydrogen Sources

Atsushi Kobayashi*[a]

[a] Dr. A. Kobayashi
Department of Chemistry, Faculty of Science
Hokkaido University
North-10 West-8, Kita-ku Sapporo 060-0810, Japan
E-mail: akoba@sci.hokudai.ac.jp

Abstract: Visible-light-driven photocatalytic hydrogen (H_2) production has been extensively studied as a clean and sustainable energy resource. Although sacrificial electron donors (SEDs) are commonly used to evaluate photocatalytic activity, their irreversible decomposition forces charge separation, which disrupts the inherent dual productivity of photocatalysis, that is, the formation of both the reduction and oxidation products. To achieve highly efficient photoinduced charge separation without SED decomposition, the layer-by-layer assembly of redox-active photosensitizing dyes and electron mediators through Zr^{4+}-phosphonate bonds has been extensively studied as an artificial mimic of the electron transport chain in natural photosynthesis. This concept paper presents an overview of photoredox cascade catalytic (PRCC) systems comprising multiple Ru(II)-trisbipyridine-type dyes and mediator layers on Pt-loaded TiO_2 nanoparticles for H_2 production from redox reversible electron donors (RREDs). The PRCC structure-activity relationship for photocatalytic H_2 production is briefly discussed in terms of layer thickness, surface structure and modification, and cooperativity with molecular oxidation catalysts. Finally, new insights into the design of efficient dual-production photocatalysts based on the PRCC structure are presented.

Introduction

Hydrogen is a key clean energy material for a next-generation sustainable society. Water splitting generates H_2 without negative environmental impact and has therefore been extensively studied.[1]



Atsushi Kobayashi was born in Nagano Prefecture, Japan, in 1978. He received his Ph.D. degree under the supervision of Prof. H. Kitagawa at Kyushu University in 2006. After working as a postdoctoral fellow in Prof. H. Kitagawa's group at Kyushu University, he joined the Faculty of Science, Hokkaido University as an Assistant Professor in 2007 and was promoted to Associate Professor in 2014. He was a PRESTO (Precursory Research for Embryonic Science and Technology) fellow at the Japan Science and Technology Agency from 2012 to 2016. His research interests include the photochemistry of metal-complex assemblies on solid surfaces.

Since the pioneering work on TiO_2 photoanodes by Honda and Fujishima,[2] semiconductor photocatalysts that split water into H_2 and O_2 under sunlight irradiation have attracted considerable attention because they enable the direct conversion of sunlight into chemical energy, which is analogous to natural photosynthesis.[3] Although numerous remarkable developments in this field have been reported,[4] the practical application of photocatalytic water splitting as the H_2 source remains challenging due to insufficient solar-to-hydrogen conversion efficiencies.[5] In addition, O_2 which is a byproduct of water splitting, is abundant on earth and therefore has limited industrial value. Another issue is that water splitting does not generate organic compounds necessary for human life. In other words, solar water splitting reaction can provide clean energy resource, H_2 without any environmental impact, but it is not a direct means of replacing fossil fuels used as various carbon resources. To address these issues, dual-productive photocatalysts that produce both H_2 and valuable organic chemicals from sustainably available biomass resources under sunlight irradiation are required.

It is widely accepted that in an ideal photocatalytic process, a photo-generated electron-hole pair should separate spontaneously and proceed to the reduction and oxidation sites, respectively (Figure 1).[3-5] After several charge-separation cycles, a sufficient number of electrons and holes with suitable reduction and oxidation potentials is accumulated, and two different reactions occur to provide the reduction and oxidation

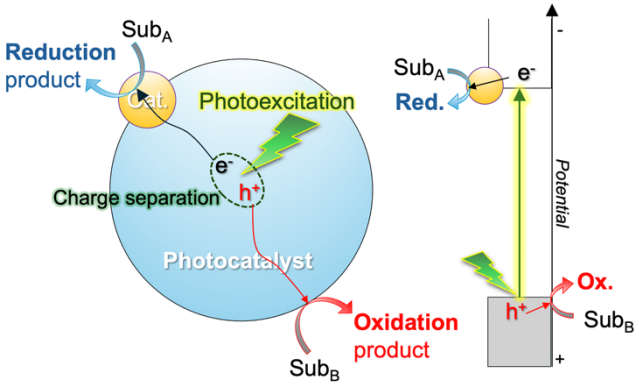


Figure 1. Schematic illustration and energy diagram of a co-catalyst-loaded semiconductor photocatalyst for the production of reduction and oxidation products.

products, namely H_2 and O_2 as the two-electron reduced and four-electron oxidized products, respectively. However, this *dual productivity* of the photocatalytic reaction is lost when a sacrificial electron donor/acceptor (SED/A) is used to facilitate photo-induced charge separation.[6] This is because sacrificial reagents decompose rapidly and irreversibly after the electron transfer reaction. Thus, achieving efficient photo-induced charge separation while avoiding the irreversible decomposition of the sacrificial reagent is crucial for obtaining both the reduced and oxidized products from photocatalytic reactions.

In natural photosynthesis, the electron transport chain, consisting of multiple redox-reversible electron mediators (RREMs) arranged to construct a multistep redox potential cascade structure, plays a key role in the highly efficient photoinduced charge separation process (Figure 2a).[7] The reverse electron transfer reaction in this chain is effectively suppressed, because appropriate RREM sequences minimize the possibility of charge-recombination reactions occurring by spatially separating photoexcited electron and hole at two terminals. Furthermore, the reorganization energies of RREMs are small enough to put the reverse electron transfer reaction into the Marcus inverted region.

In contrast, in most water-splitting photocatalytic systems entailing two-step photoexcitation by O_2 and H_2 evolving photocatalysts, referred to as Z-scheme water splitting, only one RREM is utilized to transfer electrons from the former the latter photocatalyst (Figure 2b).[8] This simplified electron transport mechanism based on the reversible redox cycle of RREM (RREMox/RREMred) causes undesired but thermodynamically favorable back reactions at the RREM-photocatalyst interface. For example, the photoexcited electron must be consumed by proton reduction at the H_2 evolving photocatalyst; however, the electrons are readily transferred to the one-electron-oxidized RREM (=RREMox) because the driving force of the back reaction is sufficiently large. Thus, considering that most artificial systems, including Z-scheme water-splitting photocatalysts, suffer from back reactions,[9] the fabrication of multistep redox cascade structure that facilitates one-way electron transfer at photocatalyst surface is highly desirable.

Dye-sensitized solar cells (DSSCs) are another notable solar energy conversion device and have been extensively studied since the early 1990s.[10] The reduction and oxidation reactions of the electrolyte, which correspond to the RREM in the Z-scheme photocatalysis, occur on the surface of the spatially separated two electrodes (Figure 3a, typically, a transparent glass-conducting cathode and dye-sensitized porous TiO_2 photoanode, respectively).[11] Since the suppression of the back electron transfer reaction between the photoexcited dye on the semiconductor surface and RREM is crucial to improve the photo-induced charge separation efficiency of DSSC as in the case of Z-scheme water splitting photocatalysis, various techniques have been extensively studied so far, ranging from introduction of donor/acceptor moieties to molecular photosensitizer to molecular assemblies on the semiconductor electrode to produce a redox potential cascade structure.[12] Furthermore, dye-sensitized photoelectrochemical cells (DSPECs) for water splitting have been developed by incorporation of molecular catalysts to dye-sensitized photoelectrodes (Figure 3b).[13] Although these interesting works on DSSCs and DSPECs clearly indicate that molecular

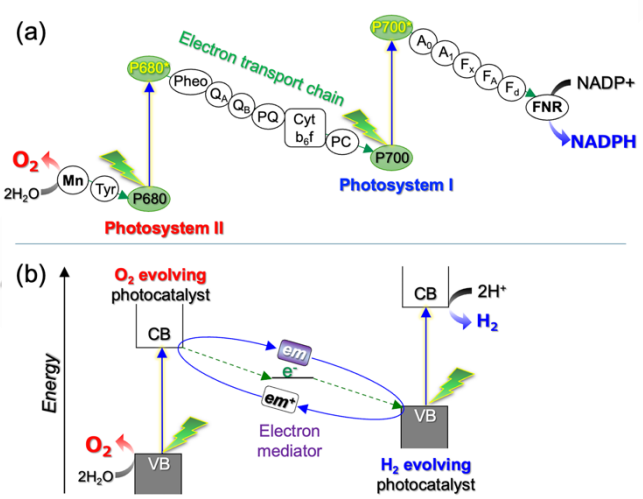


Figure 2. (a) A simplified Z-scheme of the light reactions in natural photosynthesis redrawn from ref.[7b]. (b) Schematic energy diagram of a Z-scheme water splitting photocatalysis with a single RREM.

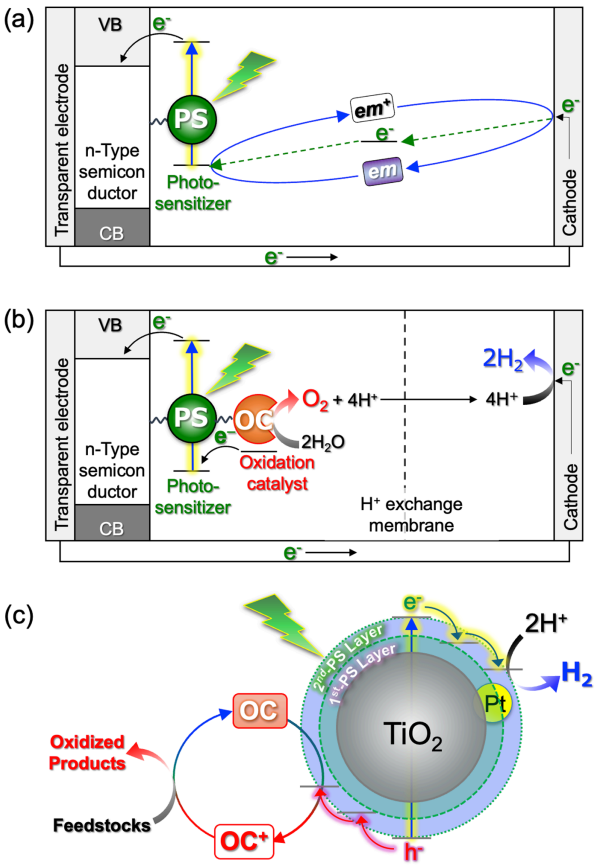


Figure 3. Schematic illustrations of (a) dye-sensitized solar cell (DSSC), (b) water-splitting dye-sensitized photoelectrochemical cell (DSPEC), and (c) photoredox cascade catalyst (PRCC).

assembly on the semiconductor surface to produce redox cascade structure should be promising strategy for solar-energy conversion, such molecular assemblies have had little application in the particulate semiconductor photocatalysis.[14]

Considering above, we have recently developed photoredox cascade catalysts (PRCC, Figure 3c) by assembling functional molecules on the surface of particulate semiconductor photocatalysts not only to artificially mimic the electron transport chain for efficient charge separation with RREM, but also to achieve dual productive photocatalytic reaction, that is, solar H_2 production with oxidative conversion of feedstocks like biomass. Thus, in this paper, the first concept overviewed herein is the photo-induced charge separation by RREMs in H_2 evolution dye-sensitized photocatalytic particulate systems. Second, the importance of the multistep redox cascade structure in photocatalytic H_2 evolution using SED/RREM is briefly discussed. Finally, further developments toward achieving dual-productive photocatalysis by providing two value-added reduction and oxidation products are reviewed.

H_2 Production under Non-sacrificial Conditions

Various SED/As have been widely utilized to evaluate the photocatalytic activity of the half (H_2 or O_2) reactions in water splitting.[6] Although this method offers valuable insights into electron transfer kinetics, information regarding back reactions and the bottleneck issue in Z-scheme water splitting photocatalysis cannot be obtained in this way. In other words, a photocatalyst determined to be optimal based on studies using sacrificial reagents may not be suitable for the construction of dual-productive photocatalytic systems. Thus, photocatalytic activity should ideally be evaluated using not only sacrificial reagents but also RREMs. Pioneering work based on dye-sensitized photocatalytic H_2 production from a non-sacrificial RRED using a Ru(II)-dye-sensitized Pt-intercalated $K_4Nb_6O_{17}$ layered semiconductor was performed by Mallouk *et al.* in 1991 (Figure 4).[15] The apparent quantum yield (AQY) in KI aq. for the production of H_2 and I_3^- as the reduction and oxidation products, respectively, was estimated to be 0.3% at the initial stage. This value was two orders of magnitude lower than that reported for an analogous Ru(II)-dye-sensitized Pt-loaded TiO_2 catalyst operated under SED conditions (28%).[16] This significant decrease in the AQY of the non-SED photocatalytic system indicates that the dominant deactivation pathway therein involves charge-recombination between the injected electron and one-electron oxidized RRED. The authors additionally highlighted the importance of optimizing the co-catalyst assembly; excessive loading of the Pt co-catalyst on the exterior surface of layered niobates had a detrimental effect on the H_2 production rate due to the backward product decomposition reaction between H_2 and I_3^- to reform $2H^+$ and $3I^-$.

Photosensitizing Dye Layering

As mentioned in the previous section, the suppression of back reactions, including charge recombination and product

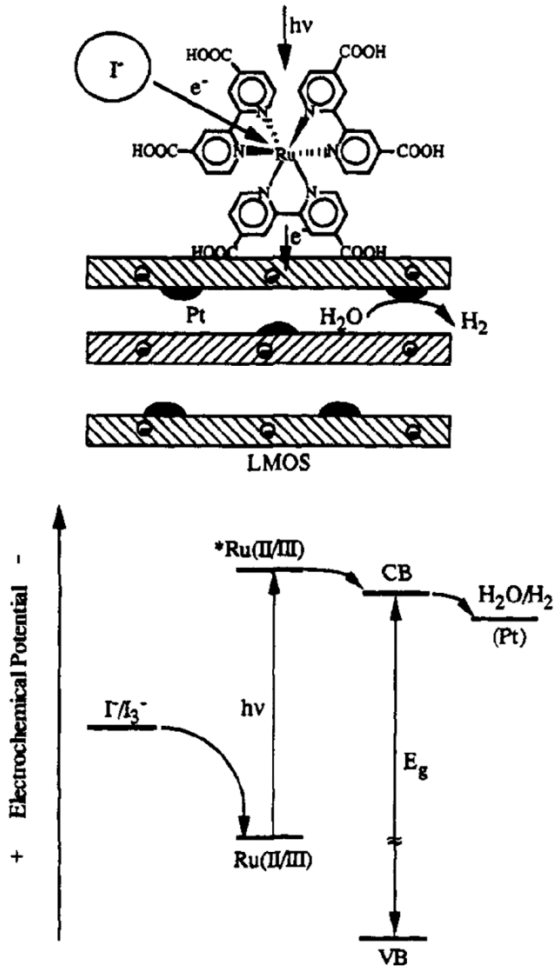


Figure 4. Schematic structure and energy diagram of Ru(II)-dye sensitized Pt-intercalated layered niobate for HI photolysis. Reproduced from ref.[15a] copyright (1991) with permission from American Chemical Society.

decomposition, is a critical issue that must be overcome. In a photoelectrochemical cell consisting of two different (photo)electrodes, the latter issue is circumvented because the two electrodes are physically separated.[17] In contrast, particulate photocatalysts are designed to generate both the reduction and oxidation products at the same surface, making it difficult to utilize RREMs as the electron/hole source. This implies that two distinct oxidation and reduction sites must be constructed within the overall assembly. The intercalation of H_2 evolution co-catalysts in the interlayer space of layered semiconductors was developed to inhibit the back reaction (water formation) at the co-catalyst surface, as mentioned above.[18] Covering the surface of noble-metal catalysts with a thin-layer of metal oxides, such as core-shell structured co-catalysts, has also been widely applied in water-splitting particulate photocatalysts; the thin oxide layer acts as a physical barrier against O_2 penetration to the co-catalyst surface, effectively suppressing the back water formation reaction.[19] However, the primary focus of such methods is molecular filtering, which has minimal impact on the light absorption and charge separation efficiencies.

Thus, for comprehensive optimization, the barrier against the penetration of undesired molecules to the photocatalyst surface should be composed of efficient light absorbers and redox-active molecules that contribute to photo-induced charge separation. To this end, we fabricated tris-bipyridine-type Ru(II) photosensitizing dye multilayers on the surface of semiconductor nanoparticles[20,21] using the layer-by-layer method based on the water-stable Zr^{4+}-phosphonate coordination bond (Figure 5).[22,23] This approach was pursued based on several excellent studies on molecular assemblies containing Ru(II)-photosensitizing dyes on electrode surfaces, which demonstrated that these systems exhibited extremely long-lived photo-induced charge-separated states[24] and one-directional excited energy transfer.[25] In addition, the wide controllability of the redox potential and light absorption wavelength of Ru(II) dyes through systematic ligand functionalization enabled us to artificially mimic the redox cascade structure of the electron transport chain in natural photosynthesis. The layer-by-layer immobilization of three different Ru(II) dyes (**RuP^6**, **RuP^4** and **RuCP^2** as the inner, middle and outer dyes, respectively) was realized through Zr^{4+}-phosphonate bonds on the surface of the H_2-evolving Pt-TiO_2 nanoparticles to produce single-, dual- and triple-dye sensitized Pt-TiO_2 nanoparticle photocatalysts (**SDSP** = **RuCP^2**@Pt-TiO_2, **DDSP** = **RuCP^2**-Zr-**RuP^6**@Pt-TiO_2, **TDSP** = **RuCP^2**-Zr-**RuP^4**-Zr-**RuP^6**@Pt-TiO_2, Figure 5).[20] An important finding was that the photocatalytic H_2 evolution activities in SED (AA = ascorbic acid) and RRED (KI) followed dissimilar trends. The estimated AQY in 0.5 M AA for 6 h irradiation decreased in the order of **DDSP** > **SDSP** > **TDSP** (entries 1a, 2a, and 3a in Table 1, 3.77%, 1.35%, and 0.64%, respectively).[20] Although the AQY in 0.5 M KI aq. was more than two-orders of magnitude lower than that in AA owing to back reactions, it increased markedly when the dye layer thickness was increased (entries 1b, 2b, and 3b in Table 1, 0.0024%, 0.018%, and 0.0458% for **SDSP**, **DDSP**, and **TDSP**, respectively).[21] In both AA and KI aq., the total amount of Ru(II) dye in each reaction was constant (100 μM), suggesting that the significant difference among the three photocatalysts with distinct dye layer structures did not originate from the light absorption efficiency, but from the photo-induced charge-separation efficiency. The largest difference between these two conditions was observed for **SDSP**, where the AQY decreased by a factor of approximately 560 when AA was replaced by KI, and ultimately, its photocatalytic activity in KI aq. was quenched (entry 1b in Table 1, turnover number of photosensitizer, PS TON < 0.28). The smallest difference was noted for **TDSP** (factor of 14), and H_2 evolved photocatalytically even in KI aq. (entry 3b in Table 1, TON = 5.44). Thus, the increased thickness of the Ru(II)-dye layer effectively suppressed the back reactions involving the RRED by acting as a physical barrier against penetration of the oxidized product I_3^- to the Pt-co-catalyst surface. This is supported by the doubling of the AQY (entry 3c in Table 1, 0.10%) when the size of the Pt co-catalyst was reduced from 6 to 3 nm in diameter, achieved by decreasing the Pt loading amount from 5 to 1 wt% in the photo-deposition process.[16] Furthermore, the spatially charge-separated state is preferentially generated by electron injection to TiO_2, followed by hole migration from the inner to the outer dye layers according to the photoredox cascade structure, which suppresses charge-recombination. Overall, the results suggested that the best-performing photocatalyst under SED conditions may not be optimal under RREM conditions.

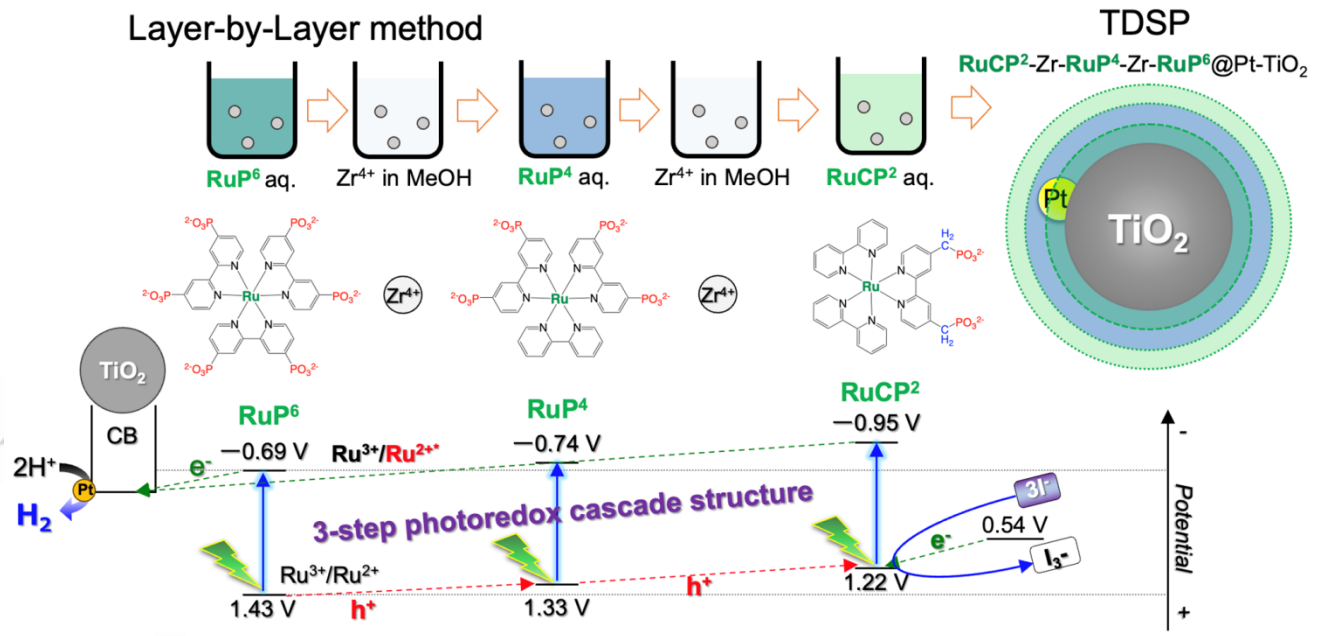


Figure 5. Schematic representations of (top) stepwise layer-by-layer synthesis and (bottom) three-step photoredox cascade structure of triple-dye sensitized Pt-TiO_2 photocatalyst (TDSP = **RuCP^2**-Zr-**RuP^4**-Zr-**RuP^6**@Pt-TiO_2) for photocatalytic H_2 evolution in KI aq.

Table 1. Results of photocatalytic H_2 production by Ru(II)-dye-multilayered Pt-TiO_2 nanoparticle photocatalysts.[a]

Entry	Photocatalyst	Composition of photocatalyst	Pt / wt%	Electron donor(s)	λ / nm	pH	Evolved H_2 / μmol	PS TON / Time	AQY / %	Ref.
1a	**SDSP**	**RuCP²**@Pt-TiO_2	5	0.5 M AA	470 ± 10	2	92.0	368 / 6 h	1.35	20
1b	**SDSP**	**RuCP²**@Pt-TiO_2	5	0.5 M KI	470 ± 10	2	0.07	0.28 / 6 h	0.002	21
2a	**DDSP**	**RuCP²**-Zr-**RuP⁶**@Pt-TiO_2	5	0.5 M AA	470 ± 10	2	256	1022 / 6 h	3.77	20
2b	**DDSP**	**RuCP²**-Zr-**RuP⁶**@Pt-TiO_2	5	0.5 M KI	470 ± 10	2	0.53	2.1 / 6 h	0.018	21
2c	**DDSP**	**RuCP²**-Zr-**RuP⁶**@Pt-TiO_2	1	0.5 M KI	470 ± 10	2	0.84	3.4 / 6 h	0.028	21
3a	**TDSP**	**RuCP²**-Zr-**RuP⁴**-Zr-**RuP⁶**@Pt-TiO_2	5	0.5 M AA	470 ± 10	2	43.4	174 / 6 h	0.64	20
3b	**TDSP**	**RuCP²**-Zr-**RuP⁴**-Zr-**RuP⁶**@Pt-TiO_2	5	0.5 M KI	470 ± 10	2	1.36	5.44 / 6 h	0.0458	21
3c	**TDSP**	**RuCP²**-Zr-**RuP⁴**-Zr-**RuP⁶**@Pt-TiO_2	1	0.5 M KI	470 ± 10	2	2.98	11.9 / 6 h	0.100	21
4	**P-DDSP**	**RuCP⁶**-Zr-**RuP⁶**@Pt-TiO_2	1	0.5 M KI	470 ± 10	2	8.8	33.2 / 6 h	0.30	26
5	**Zr-DDSP**	Zr-**RuCP⁶**-Zr-**RuP⁶**@Pt-TiO_2	1	0.5 M KI	470 ± 10	2	16.1	64.5 / 6 h	0.54	26
6a	**Zr-DDSP**	Zr-**RuCP⁶**-Zr-**RuP⁶**@Pt-TiO_2	1	16.4 mM $[Co(bpy)_3]^{2+}$	460 ± 15	2	15.2	60.7 / 6 h	0.523	34
6b	**Zr-DDSP**	Zr-**RuCP⁶**-Zr-**RuP⁶**@Pt-TiO_2	1	0.5 M H_2QSK	460 ± 15	2	8.33	33.3 / 6 h	0.280	34
7a	**PRCC-1**	**HCRu**-Zr-**RuCP⁶**-Zr-**RuP⁶**@Pt-TiO_2	1	16.4mM $[Co(bpy)_3]^{2+}$	460 ± 15	2	28.9	116 / 6 h	0.994	34
7b	**PRCC-1**	**HCRu**-Zr-**RuCP⁶**-Zr-**RuP⁶**@Pt-TiO_2	1	0.5 M H_2QSK	460 ± 15	2	12.6	50.5 / 6 h	0.433	34
8	**PRCC-2**	**HCFe**-Zr-**RuCP⁶**-Zr-**RuP⁶**@Pt-TiO_2	1	16.4mM $[Co(bpy)_3]^{2+}$	460 ± 15	2	11.9	47.8 / 6 h	0.409	34
9a	**Zr-DDSP**	Zr-**RuCP⁶**-Zr-**RuP⁶**@Pt-TiO_2	2.5	5 mM TEMPO	460 ± 15	7	7.09	29.8 / 24 h	0.098[b]	37
9b	**Zr-DDSP**	Zr-**RuCP⁶**-Zr-**RuP⁶**@Pt-TiO_2	2.5	5 mM TEMPO, 0.1 M glycerol	460 ± 15	9	78.6	314 / 24 h	0.516[b]	37
9c	**Zr-DDSP**	Zr-**RuCP⁶**-Zr-**RuP⁶**@Pt-TiO_2	2.5	5 mM TEMPO, 0.1 M cellulose	460 ± 15	9	46.9	187 / 24 h	0.398[b]	37
9d	**Zr-DDSP**	Zr-**RuCP⁶**-Zr-**RuP⁶**@Pt-TiO_2	2.5	5 mM TEMPO, 0.1 M 2-PrOH	460 ± 15	9	21.0	84.1 / 24 h	0.155[b]	37

[a] Reaction conditions: [Ru dye] = 100 μM in total, solution vol. = 5 mL. Definition: PS TON = turn over number of photosensitizer, AQY = apparent quantum yield, AA = ascorbic acid, KI = potassium iodide, TEMPO =2,2,6,6-tetramethylpiperidine 1-oxyl, 2-PrOH = 2-propanol, **RuCP²** = $[Ru(bpy)_2(mpbpy)]^{2-}$, **RuP⁴** = $[Ru(bpy)(pbpy)_2]^{6-}$, **RuP⁶** = $[Ru(pbpy)_3]^{10-}$, **RuCP⁶** = $[Ru(mpbpy)_3]^{10-}$, bpy = 2,2'-bipyridine, H_4mpbpy = 2,2'-bipyridine-4,4'-bis(methanephosphonic acid), H_4pbpy = 2,2'-bipyridine-4,4'-bis(phosphonic acid) **HCRu** = $[Ru(CN)_6]^{4-}$, **HCFe** = $[Fe(CN)_6]^{4-}$, and H_2QSK = potassium hydroquinone sulfonate [b] AQY for initial 1 h of irradiation.

Effect of Surface Functional Groups

As mentioned, because both reduction and oxidation reactions occur on the photocatalyst surface, the construction of two spatially separated reaction sites through surface modification is highly desirable. Encasing the Pt-TiO_2 nanoparticles in a triple Ru(II)-dye layer was found to suppress back reactions with RRED, presumably because the reaction sites for proton reduction and RRED oxidation were spatially separated by this layer.[21] On the other hand, the lowest AQY under SED conditions was attained by **TDSP**, implying that the thick dye layer impeded charge-separation. To overcome this problem and promote RRED oxidation, thinner dual-dye layered photocatalysts with phosphonate or Zr^{4+}-phosphonate surface groups (Figure 6, **P-DDSP** = **RuCP⁶**-Zr-**RuP⁶**@Pt-TiO_2 and **Zr-DDSP** = Zr-**RuCP⁶**-Zr-**RuP⁶**@Pt-TiO_2) were fabricated by

replacing the outer **RuCP²** dye by its six-methanephosphonate-functionalized analogue, **RuCP⁶**.[26] Despite the comparable Ru(III)/Ru(II) redox potentials of **RuCP²** and **RuCP⁶** (1.22 and 1.15 V vs. NHE, respectively)[27] and the negligible shift therein resulting from phosphonate functionalization (< 0.04 V),[28] the three dual-dye-layered photocatalysts exhibited considerable differences in their photocatalytic H_2 evolution activities in 0.5 M KI aq.; during 6 h of irradiation, the AQY increased in the following order: **DDSP** (AQY = 0.028%) < **P-DDSP** (0.30%) < **Zr-DDSP** (0.54%, entries 2c, 4 and 5, respectively, in Table 1) This significant difference of more than 10-fold between the non-surface-functionalized **DDSP** and the two surface-functionalized photocatalysts, **P-DDSP** and **Zr-DDSP** indicates that the surface groups play an important role in promoting electron donation from the RRED iodide. Considering that two-electron donation and the formation of two bonds must occur to produce triiodide (I_3^-) as a stable oxidation product from three I^- anions,[29] the electrostatic attraction between the I^- anions and the positively charged Zr^{4+}-phosphonate groups of **Zr-DDSP** possibly resulted in the accumulation of I^- anions near the photocatalyst surface, facilitating electron donation. Although the phosphonate group is negatively charged in the protonated state, and would therefore electrostatically repel I^-, hydrogen bonding interactions with the monoprotonated phosphonate group of **P-DDSP** may have counteracted the electrostatic repulsion and facilitated the accumulation of I^- anions near the photocatalyst surface. Similar results relating to the electrostatic interaction between RRED and the photocatalyst surface have been reported,[30, 31] highlighting the importance of photocatalyst surface design for promoting only the desired reactions.

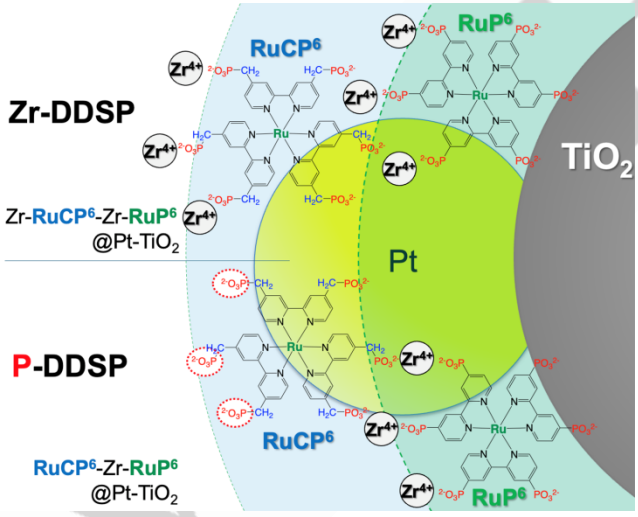


Figure 6. Schematic representation of the surface-functionalized dual-Ru(II)-dye sensitized Pt-TiO_2 photocatalysts, (top) **Zr-DDSP** and (bottom) **P-DDSP** having distinct surface functional groups.

Hole Mediator Modification

In general, a photosensitizing dye immobilized on the surface of an *n*-type semiconductor should rapidly inject photoexcited electrons into the conduction band to induce the charge-separated state. However, in cases where the photocatalyst surface effectively attracts the RREM resulting in the rapid regeneration of the photosensitizing dye, other undesired electron and/or energy transfers (e.g. from the photoexcited dye to the RREMox) can occur.[32] To minimize such undesired reactions, we immobilized the hexacyanido Ru(II) complex $[Ru(CN)_6]^{4-}$ (=**HCRu**) on the surface of **Zr-DDSP** as a visible-light transparent hole mediator (Ru(III)/Ru(II) at 0.89 V vs. NHE)[33] to form **HCRu**-Zr-**RuCP⁶**-Zr-**RuP⁶**@Pt-TiO_2 (**PRCC-1**, Figure 7)[34] as a three-step photoredox cascade catalyst.

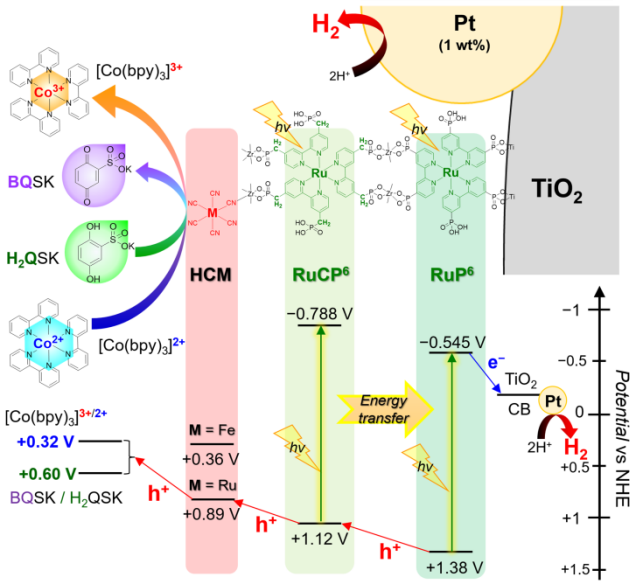


Figure 7. Schematic structure and energy diagram of the **HCRu** hole mediator immobilized on the three-step photoredox cascade catalyst, **PRCC-1**. Reproduced from ref.[29] copyright (2023) with permission from the American Chemical Society.

The AQY and PS TON values of **PRCC-1** for photocatalytic H_2 evolution during 6 h of irradiation were approximately two-fold higher than those of **Zr-DDSP** in 16.4 mM $[Co(bpy)_3]^{2+}$ aq., which is commonly used as a RREM in various Z-scheme water splitting photocatalysts[35] (entries 6a and 7a in Table 1). In contrast, the activity was drastically reduced to ~40% that of **PRCC-1** when **HCRu** was replaced by the more readily oxidizable Fe(II) analogue, $[Fe(CN)_6]^{4-}$ (**PRCC-2**, Fe(III)/Fe(II) at 0.36 V vs. NHE, entry 8 in Table 1), suggesting that the appropriate redox potential difference between the surface-immobilized **HCRu** and $[Co(bpy)_3]^{2+}$ aq. (~0.57 V)[35] is important for efficient hole transfer to (= electron donation from) the RREM. In other words, the construction of a photoredox cascade structure suitable for photo-induced electron injection into TiO_2 and subsequent hole migration from the inner **RuP⁶** dye to the $[Co(bpy)_3]^{2+}$ RRED, occurring via two layers (**RuCP⁶** and **HCRu**), played a key role in the overall photo-induced charge separation phenomenon in this system. A similar difference in activity was also observed between **PRCC-1** and **Zr-DDSP** when $[Co(bpy)_3]^{2+}$ was replaced with hydroquinone monosulfonate, which is an analog of the proton and electron mediator used in the electron transport chain of natural photosynthesis (entries 6b

and 7b in Table 1). These results suggest that extending the photoredox cascade structure based on visible-light-transparent RREMs to artificially mimic the electron transport chain in natural photosynthesis is a promising strategy for achieving highly efficient photoinduced charge separation.

Cooperation with Molecular Catalyst for Biomass Reforming

From the perspective of carbon neutrality, the use of biomass as an alternative to fossil fuels is highly desirable. Biomass photoreforming is a promising reaction that provides both a clean energy resource in the form of H_2 and valuable chemicals as a result of water reduction and biomass oxidation.[36] As discussed in the previous section, **PRCC-1** photocatalytically generates H_2 coupled with the oxidation of various RREMs.[34] This result motivated us to further develop a new photoredox cascade catalytic system by replacing the surface-immobilized **HCRu** hole mediator with an alcohol-oxidation molecular catalyst, namely, 2,2,6,6-tetramethylpiperidine 1-oxyl (TEMPO•), to achieve dual productive photocatalysis, that is, to provide both H_2 and value-added chemicals derived from biomass oxidation (Figure 8).[37]

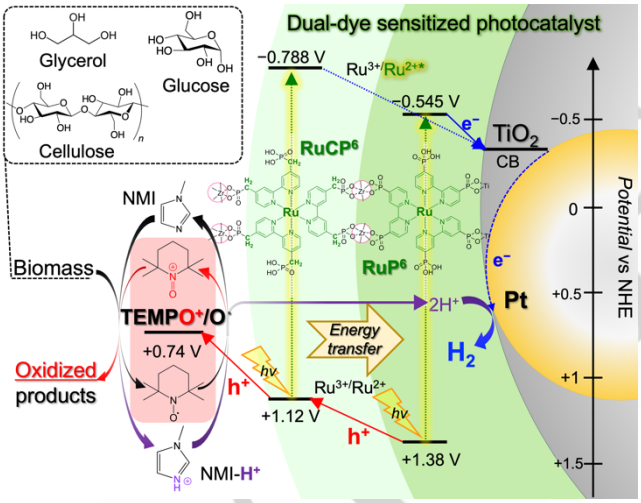


Figure 8. Schematic representation of photoredox cascade catalytic system comprising H_2-evolving **Zr-DDSP** and TEMPO• molecular catalyst for biomass oxidation. Reproduced from ref.[32] copyright (2023) with permission from Wiley-VCH.

In 5 mM TEMPO aq., **Zr-DDSP** evolved H_2 under blue light irradiation, and the estimated PS TON was approximately 30 after 6 h of irradiation (entry 9a in Table 1), indicating that TEMPO• underwent oxidation as a result of the photocatalytic production of H_2 by **Zr-DDSP**. The PS TON increased up to 314 with the addition of 0.1 M glycerol and 50 mM N-methylimidazole (entry 9b in Table 1), suggesting that glycerol was oxidized by one-electron oxidized $TEMPO^+$, facilitated by N-methylimidazole as the proton-acceptor (base) to afford the oxidized glycerol species and regenerate the TEMPO• radical. In the ^{13}C NMR spectrum of the reaction supernatant, several new signals were observed, including the characteristic signal of the carboxylate species at 179 ppm, suggesting the successful oxidation of glycerol. Notably, the estimated PS TON in an aqueous dispersion of insoluble cellulose (0.1 M as the cellulose monomer unit) was two-fold higher than that in 0.1 M 2-propanol aq. (Table 1, entries 9c and 9d). Considering that sterically bulky TEMPO• can selectively oxidize primary alcohols in the presence of suitable oxidants such as O_2,[38] a plausible origin of the higher PS TON in the cellulose dispersion than in 2-propanol aq. is that the surface primary hydroxyl groups at the C6 position of the cellulose polymer was oxidized by the photochemically produced $TEMPO^+$, as evidenced by the characteristic IR band of the carboxylate group at 1607 cm^{-1}. These results demonstrate that **Zr-DDSP** and TEMPO• function cooperatively to realize the photocatalytic production of H_2 and oxidized carboxylate species from biomass resources such as cellulose and glycerol.

Summary and Outlook

Traditionally, photocatalytic activity has been evaluated in the presence of sacrificial agents. However, irreversible decomposition of the sacrificial agent forces charge separation, which disrupts the inherent dual productivity of photocatalysis produces two beneficial reduction and oxidation products. To obtain both redox products without the use of sacrificial agents, the electron-hole pairs generated as a result of light absorption must be efficiently separated to drive the two redox reactions without competition. In this regard, to artificially mimic the electron transport chain in natural photosynthesis, the layer-by-layer assembly of photosensitizing dyes and redox-active electron mediators by Zr^{4+}-phosphonate coordination bonds has been extensively studied, not only on semiconductor electrode surfaces but also on nanoparticle photocatalyst surfaces. In this concept paper, our recent progress on PRCC systems for H_2 production was briefly reviewed. The salient findings are as follows:

1. The dissimilar trends in the photocatalytic H_2 production activities of the single-, dual-, and triple-dye-sensitized Pt-TiO_2 photocatalysts (**SDSP**, **DDSP** and **TDSP**) under SED (AA) and RRED (KI) conditions indicate that the best-performing photocatalyst under SED conditions is not necessarily the best under RREM conditions.
2. Photocatalytic H_2 production using aqueous iodide was improved by the formation of a thicker (dual and triple) dye layer, plausibly because the dye layer extracted holes from the outer surface after photoelectron injection and acted as a barrier that prevented RRED penetration to the electron-injected semiconductor surface.
3. The surface composition of the photosensitizing dye layer is an important factor that significantly affects the photocatalytic H_2 production activity; the positively charged Zr^{4+}-phosphonate groups of **Zr-DDSP** electrostatically attract iodide anions, thereby facilitating electron donation, followed by stable I_3^- formation.
4. The immobilization of visible-light-transparent **HCRu** to construct a three-step photoredox cascade structure (**PRCC-1**) further enhanced the photocatalytic H_2

production activity, attaining an AQY comparable to that of **SDSP** under SED conditions.

5. The combination of **Zr-DDSP** and TEMPO• as a molecular catalyst enabled dual-productive photocatalysis encompassing H_2 production coupled with biomass (cellulose and glycerol) oxidation.

These results demonstrate that cascade-structured PRCC systems that facilitate charge separation are suitable for the production of both valuable redox products via photocatalysis. Although the activity of the present system is insufficient for practical solar H_2 production, further improvements are expected to be realized through the stepwise extension of the PRCC structure entailing the assembly of redox-active photosensitizing dyes and mediators to resemble the electron transport chain in natural photosynthesis. Additionally, noble-metal-based materials should ideally be replaced by non-precious-metal counterparts. Importantly, a variety of oxidation reactions can now be coupled with photochemical H_2 production using molecular catalysts such as TEMPO•.[39] This strategy enables the simultaneous production of H_2 as well as useful oxidation products from natural carbon resources such as cellulose. Compared with water splitting Z-scheme photocatalysis, this approach can potentially replace the production of oxygen, a cheap byproduct of conventional water splitting, with that of high-value-added organic products, and thereby ameliorate the problem of high H_2 production costs. In addition, only one photoexcitation is necessary for the PRCC system to transfer the electron from oxidation to reduction site, which can increase the quantum yield from the 50% limit for Z-scheme photocatalysis to nearly 100%. Further studies on the stepwise extension of the PRCC structure, its fine-tuning, and cooperativity with various molecular catalysts are in progress.

Acknowledgements

The author deeply thanks Prof. K. Sada (Hokkaido Univ.) for his warmful support in the development of laboratory environment. This study was supported by the ENEOS Hydrogen Trust Fund, the Casio Science Promotion Foundation, the Iwatani Naoji Foundation, and JSPS KAKENHI (grant numbers 23H01969 and 22K19039).

Keywords: Photocatalysis • Dye sensitization • Charge separation • Biomass reforming • Water splitting

[1] F. Dawood, M. Anda, G.M. Shafiullah, *Int. J. Hydrogen Energy* **2020**, *45*, 3847.

[2] A. Fujishima, K. Honda, *Nature* **1972**, *238*, 37.

[3] (a) Y. Ma, X. Wang, Y. Jia, X. Chen, H. Han, C. Li, *Chem. Rev.* **2014**, *114*, 9987. (b) Q. Wang, K. Domen, *Chem. Rev.* **2020**, *120*, 919. (c) X. Fang, S. Kalathil, E. Reisner, *Chem. Soc. Rev.* **2020**, *49*, 4926.

[4] (a) D. G. Nocera, *Acc. Chem. Res.* **2012**, *45*, 767. (b) Q. Wang, T. Hisatomi, Q. Jia, H. Tokudome, M. Zhong, C. Wang, Z. Pan, T. Takata, M. Nakabayashi, N. Shibata, Y. Li, I. D. Sharp, A. Kudo, T. Yamada, K. Domen, *Nat. Mater.* **2016**, *7*, 611. (c) M. Okamura, M. Kondo, R. Kuga, Y. Kurashige, T. Yanai, S. Hayami, V. K. K. Praneeth, M. Yoshida, K. Yoneda, S. Kawata, S. Masaoka, *Nature* **2016**, *530*, 465. (d) T. Takata, J. Jiang, Y. Sakata, M. Nakabayashi, N. Shibata, V. Nandal, K. Seki, T. Hisatomi, K. Domen, *Nature* **2020**, *581*, 411.

[5] (a) H. Inoue, T. Shimada, Y. Kou, Y. Nabetani, D. Masui, S. Takagi,, H. Tachibana, *ChemSusChem* **2011**, *4*, 173. (b) S. Chen, T. Takata, K. Domen, *Nat. Rev. Mater.* **2017**, *2*, 17050.

[6] Y. Pellegrin, F. Odobel, *C. R. Chime.* **2017**, *20*, 283.

[7] (a) K. N. Ferreira, T. M. Iverson, K. Maghlaoui, J. Barber, S. Iwata, *Science* **2004**, *303*, 1831. (b) K. J. F. Govindjee, J. Messinger, J. Whitmarsh, *Photosystem II. In Encyclopedia of Life Sciences*, **2010**, Wiley.

[8] (a) Y. Wang, H. Suzuki, J. Xie, O. Tomita, D. J. Martin, M. Higashi, D. Kong, R. Abe, J. Tang, *Chem. Rev.* **2018**, *118*, 5201.

[9] D. Govindjee, D. Shevela, L, O, Björn, *Photosynth. Res.* **2017**, *133*, 5.

[10] (a) B. O'Regan, M. Grätzel, *Nature* **1991**, *353*, 737. (b) A. Hagfeldt, M. Grätzel, *Acc. Chem. Res.* **2000**, *33*, 269.

[11] (b) F. Bella, C. Gerbaldi, C. Barolo, M. Grätzel, *Chem. Soc. Rev.* **2015**, *44*, 3431.

[12] (a) A. Hagfeldt, G. Boschloo, L. Sun, L. Kloo, H. Pettersson, *Chem. Rev.* **2010**, *110*, 6595. (b), B. Bozic-Weber, E. C. Constable, C. E. Housecroft, *Coord. Chem. Rev.* **2013**, *257*, 3089. (c) J. C. Wang, S. P. Hill, T. Dilbeck, O. O. Ogunsolu, T. Banerjee, K. Hanson, *Chem. Soc. Rev.* **2018**, *47*, 104. (d) A. Arcidiacono, B. Hanks, K. Hanson, *ACS Appl. Opt. Mater.* **2023**, *1*, 1156-1168.

[13] (a) J. R. Swierk, T. E. Mallouk, *Chem. Soc. Rev.* **2013**, *42*, 2357. (b) D. L. Ashford, M. K. Gish, A. K. Vannucci, M. K. Brennaman, J. L. Templeton, J. M. Papanikolas, T. J. Meyer, *Chem. Rev.* **2015**, *115*, 13006. (c) Z. Yu, F. Li, L. Sun, *Energy Environ. Sci.* **2015**, *8*, 760. (c) A. Kobayashi, S. Takizawa, M. Hirahara, *Coord. Chem. Rev.* **2022**, *467*, 214624.

[14] (a) J. Warnan, J. Willkomm, J. N. Ng, R. Godin, S. Prantl, J. R. Durrant, E. Reisner, *Chem. Sci.* **2017**, *8*, 3070. (b) S. Nishioka, K. Hojo, L. Xiao, T. Gao, Y. Miseki, S. Yasuda, T. Yokoi, K. Sayama, T. E. Mallouk, K. Maeda, *Sci. Adv.* **2022**, *8*, eadc9115.

[15] (a) Y. Kim, S. Salim, M. J. Huq, T. E. Mallouk, *J. Am. Chem. Soc.* **1991**, *113*, 9561. (b) Y. Kim, S. J. Atherton, E. S. Brigham, T. E. Mallouk, *J. Phys. Chem.* **1993**, *97*, 11802.

[16] E. Bae, W. Choi, *J. Phys. Chem. B.* **2006**, *110*, 14792.

[17] (a) D. L. Ashford, M. K. Gish, A. K. Vannucci, M. K. Brennaman, J. L. Templeton, J. M. Papanikolas, T. J. Meyer, *Chem. Rev.* **2015**, *115*, 13006. (b) E. A. Gibson, *Chem. Soc. Rev.* **2017**, *46*, 6194.

[18] K. Sayama, A. Tanaka, K. Domen, K. Maruya, T. Onishi, *J. Phys. Chem.* **1991**, *95*, 1345.

[19] K. Maeda, K. Teramura, D. Lu, N. Saito, Y. Inoue, K. Domen, *J. Phys. Chem. C.* **2007**, *111*, 7554.

[20] S. Furugori, A. Kobayashi, A. Watanabe, M. Yoshida, M. Kato, *ACS Omega* **2017**, *2*, 3901.

[21] N. Yoshimura, A. Kobayashi, W. Genno, T. Okubo, M. Yoshida, M. Kato, *Sustainable Energy Fuels,* **2020**, *4*, 3450.

[22] L. A. Vermeulen, J. L. Snover, L. S. Sapochak, M. E. Thompson, *J. Am. Chem. Soc.* **1993**, *115*, 11767.

[23] T. Ishida, K. Terada, K. Hasegawa, H. Kuwahata, K. Kusama, R. Sato, M. Nakano, Y. Naitoh, M. Haga, *Appl. Surf. Sci.* **2009**, *255*, 8824.

[24] B. H. Farnum, K.-R. Wee, T. J. Meyer, *Nat. Chem.* **2016**, *8*, 845.

[25] K. Hanson, D. A. Torelli, A. K. Vannucci, M. K. Brennaman, H. Luo, L. Alibabaei, W. Song, D. L. Ashford, M. R. Norris, C. R. K. Glasson, J. J. Concepcion, T. J. Meyer, *Angew. Chem. Int. Ed.* **2012**, *51*, 12782.

[26] N. Yoshimura, A. Kobayashi, M. Yoshida, M. Kato, *Chem. Eur. J.* **2020**, *26*, 16939.

[27] K. Hanson, M. K. Brennaman, A. Ito, H. Luo, W. Song, K. A. Parker, R.Ghosh, M. R. Norris, C. R. K. Glasson, J. J. Concepcion, R. Lopez, T. J. Meyer, *J. Phys. Chem. C* **2012**, *116*, 14837.

[28] M. R. Norris, J. J. Concepcion, C. R. K. Glasson, Z. Fang, A. M. Lapides, D. L. Ashford, J. L. Templeton, T. J. Meyer, *Inorg. Chem.* **2013**, *52*, 12492.

[29] L. Troian-Gautier, M. D. Turlington, S. A. M. Wehlin, A. B. Maurer, M. D. Brady, W. B. Swords, G. J. Meyer, *Chem. Rev.* **2019**, *119*, 4628.

[30] N. Yoshimura, A. Kobayashi, T. Kondo, R. Abe, M. Yoshida, M. Kato, *ACS. Appl. Energy Mater.* **2021**, *4*, 14352.

[31] (a) G. B. Saupe, T. E. Mallouk, W. Kim, R. H. Schmehl, *J. Phys. Chem. B.* **1997**, *101*, 2508. (b) S. Nishioka, K. Hojo, L. Xiao, T. Gao, Y. Miseki, S. Yasuda, T. Yokoi, K. Sayama, T. E. Mallouk, K. Maeda, *Sci. Adv.* **2022**, *8*, eadc9115.

[32] N. Yoshimura, O. Tomita, R. Abe, M. Yoshida, A. Kobayashi, *ChemCatChem* **2022**, e202201386.

[33] H. Kitano, A. Kobayashi, M. Yoshida, M. Kato, *Sustainable Energy Fuels,* **2018**, *2*, 14086.

[34] N. Yoshimura, M. Yoshida, A. Kobayashi, *J. Am. Chem. Soc.* **2023**, *145*, 6035.

[35] Y. Sasaki, H. Kato, A. Kudo, *J. Am. Chem. Soc.* **2013**, *135*, 5441.

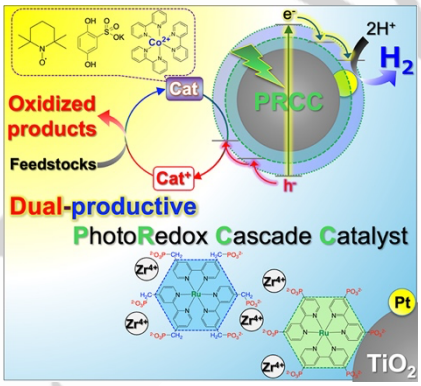
[36] M. Ashraf, N. Ullah, I. Khan, W. Tremel, S. Ahmad, M. N. Tahir, *Chem. Rev.* **2023**, *123*, 4443.

[37] A. Kobayashi, *Angew. Chem. Int. Ed.* **2023**, *62*, e202313014.

[38] R. A. Sheldon, I. W. C. E. Arends, G.-J. T. Brink, A. Dijksman, *Acc. Chem. Res.* **2002**, *35*, 774–781.

[39] A. Kobayashi, *Catal. Sci. Technol.* **2024**, *in press.*(DOI: 10.1039/D4CY00544A)

Entry for the Table of Contents



Dual-productive photocatalysis is highly desirable for supplying both hydrogen and value-added chemicals as reduction and oxidation products, respectively, for a sustainable society. An overview of photoredox cascade catalytic systems comprising Ru(II)-trisbipyridine-type dyes and electron mediators on Pt-loaded TiO_2 nanoparticles for H_2 production coupled with oxidation of redox-reversible electron mediators is presented, as well as their combination with molecular oxidation catalysts